CRYSTAL GROWTH & DESIGN

Article

pubs.acs.org/crystal

Antisolvent Crystallization and Polymorph Screening of Glycine in Microfluidic Channels Using Hydrodynamic Focusing

Venkateswarlu Bhamidi,[†,‡] Sie Huey Lee,[‡] Guangwen He,[†,‡] Pui Shan Chow,[‡] Reginald B. H. Tan,[‡,§] Charles F. Zukoski,[†] and Paul J. A. Kenis*[,†]

[†]Department of Chemical & Biomolecular Engineering, University of Illinois at Urbana−Champaign, 600 South Mathews Avenue, Urbana, Illinois 61801, United States

[‡]Institute of Chemical & Engineering Sciences, 1, Pesek Road, Jurong Island, Singapore 627833

[§]Department of Chemical and Biomolecular Engineering, National University of Singapore, 4 Engineering Drive 4, Singapore 117576

ABSTRACT: Extensive screening of the polymorph and solvate space of a given active pharmaceutical ingredient molecule is an important step in early-stage pharmaceutical product development. Thus, a significant need exists in the pharmaceutical industry for experimental techniques that facilitate the screening process with minimal material consumption and effort. Here we describe an experimental technique that facilitates antisolvent crystallization in a microfluidic channel using diffusive mixing of solutions at laminar flow interfaces (hydrodynamic flow focusing). This setup is able to produce complex and localized concentration gradients of solute and antisolvent in the microchannel, which in turn trigger the selective formation of α- and β-glycine crystals in a water−2-propanol solvent system. We correlate the polymorph selectivity observed to an empirical parameter that characterizes the supersaturation gradients. Our experiments demonstrate that characteristics of physics at the micrometer scale can be leveraged to influence the polymorph formation and habit modification of molecular crystals.

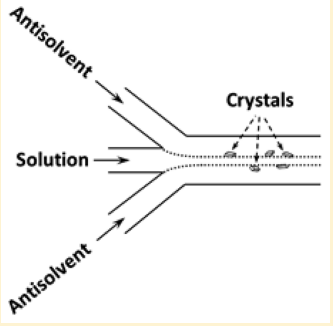

I. INTRODUCTION

The crystalline (or amorphous) state of an active pharmaceutical ingredient (API) in a solid dosage formulation strongly influences the in vivo solubility, bioavailability, and stability of a drug product. API solid forms are also carefully monitored for both intellectual property reasons and for regulatory compliance. As a result, early-stage pharmaceutical process development of a new drug molecule with a solid dosage formulation involves a significant effort toward identifying and characterizing the various crystalline forms an API and its salts can exhibit. Thus, a great need exists in the pharmaceutical industry for robust experimental techniques that facilitate rapid and thorough exploration of the polymorph and solvate space of a given API or its salt form.[1]

Due to the small amounts (usually milligram quantities) of an API available during the early stages of solid-form screening and preformulation, semimicro and high-throughput (HT) techniques are often employed to maximize the amount of information obtained regarding the polymorphic nature of API crystals with minimal time and effort.[2,3] A few such HT screening systems that use small vials or standard 96 well plates are described in the literature. Storey et al. reported the development of an automated polymorph screening system that used a 96-reactor crystallization platform in combination with automatic isolation of samples.[4] This system was capable of handling solution volumes up to 2 mL in each reactor. A similar robotic system was described by Ware and Lu, who employed an automated 96-well system that used about 5 mg of trazodone per batch toward salt screening of the API.[5]

A further reduction in material consumption and increase in throughput can be achieved by employing microfluidic technology in crystal-form screening. Crystallization in a microfluidic environment also provides us with an opportunity to take advantage of the physics of the micrometer-scale mass transport.[6] The adaptation of microfluidic technology toward crystallization applications is in the early stages of development. Earlier screening studies that used microfluidic technology have mainly focused on minimizing reagent consumption to assist high-throughput screening of protein crystallization conditions.[7,8] A few studies probed the nucleation kinetics of inorganic and organic molecular crystals using microfluidic experimental techniques.[9,10] Recently, Kenis and co-workers have described microfluidic approaches to polymorph and salt-form screening using antisolvent crystallization through free interface diffusion of solutions,[11,12] evaporative crystallization through controlled evaporation of the solvent,[13] and co-crystal screening of pharmaceutical parent compounds.[14] While these approaches all reduce the amount of material needed per condition screened, the outcome of the crystallization experiments still very much depends on the screening conditions selected, which are varied in a stepwise rather than continuous fashion.

Current HT screening methods, irrespective of scale, mostly rely on brute-force search of the parameter space and usually

Received: March 26, 2015
Revised: May 5, 2015
Published: May 7, 2015

DOI: 10.1021/acs.cgd.5b00420
Cryst. Growth Des. 2015, 15, 3299−3306

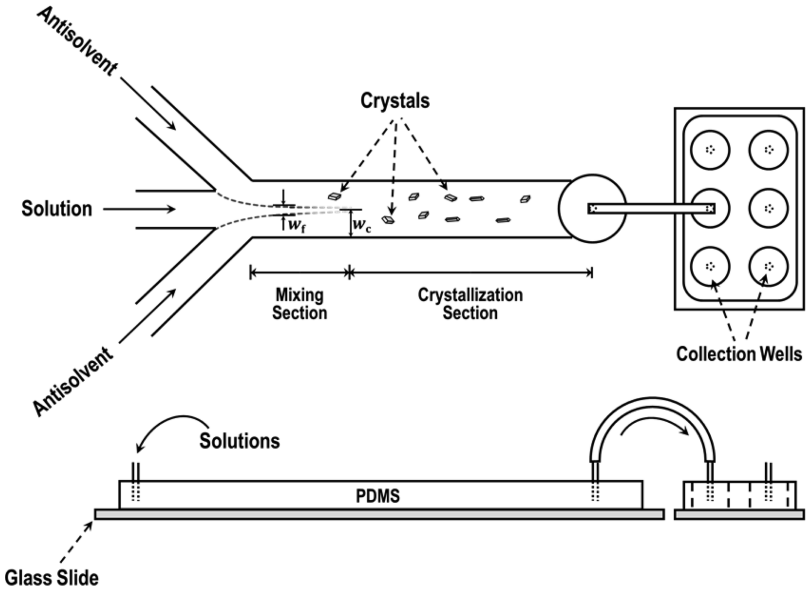

Figure 1. Schematic of the microfluidic platform for antisolvent crystallization shown in top and side views. The figure not drawn to scale. The measurements w_f and w_c indicate the width of the focused center stream and the half-width of the main channel, respectively.

lack flexibility in manipulating crystallization conditions. In these systems, the search for various polymorphs of a compound is typically conducted through batch/semibatch crystallization using temperature variation, evaporation of the solvent, and/or variation of antisolvent. Often the solution conditions screened in antisolvent crystallization consider only the final composition of the solute−solvent−antisolvent mixture in the batch. Typically solutions are mixed and are sealed inside a vial and the batch is monitored with time for solid formation. In these methods, little flexibility is offered in terms of the solution mixing process and virtually no control exists over the concentration gradients within the crystallizing (micro)batch. When crystallization is initiated through the addition of an antisolvent, the mixing time and length scales involved can drastically alter the supersaturation gradients generated in the solution. Such differences in the rate of generation of supersaturation in solution will have a significant impact on the polymorphic form in which a molecule crystallizes.[15] Building on this concept, we have designed a microfluidic system that uses the principle of hydrodynamic focusing[16] to facilitate antisolvent crystallization. In this work, we demonstrate the efficacy of our technique in generating reproducible supersaturation gradients in a crystallizing solution and in exploiting these gradients to explore the polymorphic diversity exhibited by a crystallizing compound.

II. EXPERIMENTAL SECTION

Integrated Microfluidic Mixer and Crystallizer. The experimental technique reported here relies on the principle of diffusive mixing in multistream laminar flow[17] to affect antisolvent crystallization. Figure 1 shows the schematic of the microfluidic mixer−crystallizer. In the mixing section of the device, a flowing stream of solution containing the compound of interest comes into contact with streams of antisolvent in a microchannel. Here the center stream is compressed, i.e., focused hydrodynamically, by the side streams, and narrow liquid−liquid interfaces between the solution and the antisolvent are established.[16] These streams then flow in a laminar fashion (i.e., in layers) and their molecular components (solvent and solute molecules) diffuse into each other to relax the concentration gradients. Due to the spatial variation of the concentration of species, complex supersaturation gradients are created along the mixing section. These supersaturation gradients trigger the nucleation of solute crystals under varying degrees of supersaturation. Crystals thus nucleated in different environments can potentially exhibit polymorphic diversity. The completely mixed stream containing the nucleated microcrystals then continues to flow through the channel and is diverted manually into different sampling wells in which crystals are allowed to grow. The length of the microchannel is designed such that complete mixing of the streams (as estimated by a diffusion time scale; see below) takes place before the mixed stream flows into the sampling wells. In the crystallizing portion of the channel, concentration gradients disappear and the overall supersaturation of the solution is lowered due to dilution.

The design considerations for the microfluidic chip were as follows. The inlet channels through which the solutions enter the chip were arbitrarily chosen to be of 50 μm width. To avoid any issues resulting from back-pressure during solution flow, the width of the mixing/crystallization (main) channel was set as 200 μm such that the cross-sectional area available in the main channel is more than the sum of the cross-sectional areas resulting from the three 50 μm inlet channels. The height of the channels is determined by the fabrication procedure, which in our case is 70 μm. Considering the liquid diffusivity (D) of a small molecule solute to be on the order of 10^{-9} (m^2/s),[18] the time required for a solute molecule to diffuse across a distance L of about 100 μm (half the width of the main channel) is about 10 s ($\sim L^2/D$). Thus, to ensure complete mixing, the main channel (mixing section plus crystallization section) should provide >10 s of residence time for the flowing streams. On the basis of this estimate, we designed the length of the main channel to be 35 cm and chose the flow rates of solutions used in experimentation such that for any given experimental condition the residence time of the center and side streams combined exceeded 10 s.

Fabrication of the Microfluidic Device. The crystallization platforms used in our experiments were produced using standard soft-lithographic methods.[19] In short, a transparency mask of the desired design was generated using a CAD program, and then through photolithography using negative photoresists (SU-8 2520, Microchem) this mask was used to create a master for replica molding. A working crystallization chip was created by molding poly(dimethylsiloxane) (PDMS) elastomer (GE) on the master template and binding the peeled-off PDMS replica on a glass microscope slide (Fisher) using surface plasma treatment. Several identical chips can be

DOI: 10.1021/acs.cgd.5b00420
Cryst. Growth Des. 2015, 15, 3299−3306

rapidly produced using this method. The same method was used to create a chip containing the collection wells.

Experimental Conditions and Methods. We used glycine (H_2NCH_2COOH), the simplest amino acid, in our experiments because of the rich and well-documented polymorphism of glycine crystals.[20−22] Glycine typically crystallizes into three distinct polymorphic forms at ambient conditions: α, β, and γ. We crystallized glycine (Fluka, >99.5%) by contacting aqueous glycine solutions with aqueous 2-propanol (isopropyl alcohol or IPA, Fisher Scientific, HPLC grade) solutions in the microfluidic crystallization platform. All of our experiments were performed at room temperature using saturated glycine solutions (200 mg/mL at 22 °C[23]). The concentration of antisolvent (aqueous IPA solution) was varied between 50 and 85% (v/v) IPA in DI water. The volumetric concentrations indicated for antisolvent are nominal; i.e., a 50% IPA solution was prepared by adding 5 mL of IPA to 5 mL of water. The flow rates used for glycine and IPA solutions ranged from 0.25 to 2.0 (mL/h) with antisolvent flowing in the side streams focusing the glycine solution flowing in the center.

The solutions were loaded into 5 mL disposable syringes (BD) with needles and these needles were connected to the inlet channels of the microfluidic chip using thin-walled PTFE tubing (Cole-Parmer). These syringes were then mounted on syringe pumps (Harvard Apparatus) used to control the flow rate. We manually diverted the stream exiting the microchip into various sampling wells using thin-walled PTFE tubing similar to that mentioned above. Crystals grown to about 100 μm in the sampling wells were photographed using a CCD camera (Leica DFC 320) connected to an optical microscope (Leica MZ16), typically within 1 min after the clear solution enters the sampling well. We adopted this procedure to ensure the capturing of the polymorphic selectivity before any significant solution-mediated transformation of metastable crystal forms into more stable ones can occur. Such a transformation from β-glycine to α-glycine crystals has been reported to occur over a time scale of several minutes.[24]

We established the polymorphic form of crystals that grew with various distinct habits using off-line Raman microscopy (InVia Reflex, Renishaw). The α-form exhibits a distinct signal at a wavenumber of 1035 cm^{-1} that is absent in the Raman spectrum of β-glycine crystals. Similarly, β-glycine crystals show a distinct peak at 1042 cm^{-1}. We then analyzed the optical micrographs collected from different experiments using image analysis software (Media Cybernetics, Image PRO) to determine the fractions of various polymorphs present in the total population of crystals photographed in each image. At each experimental condition, we collected multiple aliquots of the stream exiting the microfluidic device at steady state, thus producing 5−7 populations of crystals with each population containing 25−75 crystals. Our experiments mainly resulted in the formation of α- and β-glycine crystals with various habits (see below). We did not observe the formation of γ-glycine crystals.

Solubility of Glycine in Aqueous 2-Propanol Solutions. In analyzing the results from our experiments below, we relied on the solubility of α-glycine crystals in water and in water−2-propanol solutions as reported in the literature.[23−25] We estimated the supersaturation at any given solution condition by using this solubility information on α-glycine. Reliable solubility measurements on β-glycine are not readily available in the literature due to the experimental difficulties brought forth by the fast conversion of β-glycine to α-glycine.[24] The solubility of β-glycine was reported to be about 17−20% higher than that of α-glycine under similar solution conditions.[24] Due to the lack of accurate information on the solubility of β-glycine crystals, hereafter we discuss the degrees of supersaturation at various solution conditions on the basis of the solubility of α-glycine crystals. In our analysis, we use the ratio of the concentration of solute (C) to that at equilibrium (solubility, C^*) as the working definition of supersaturation for crystallization.

III. RESULTS AND DISCUSSION

Figure 2 shows an optical micrograph of a typical population of crystals in a sampling well. At least four different crystal habits

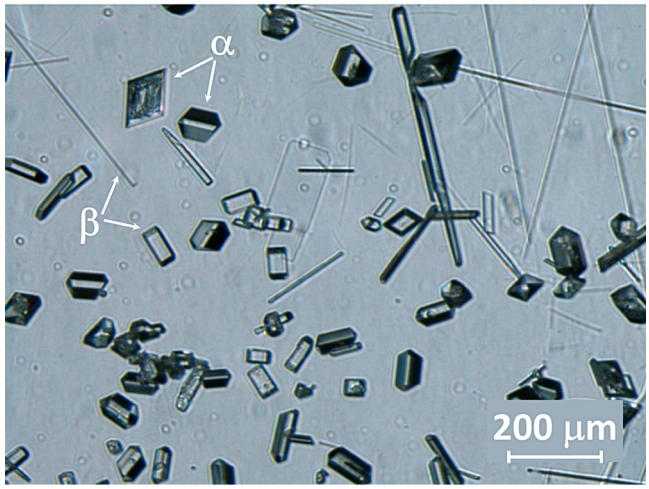

Figure 2. Typical population of glycine crystals formed in a sampling well. The four predominant habits exhibited by α- and β-forms of glycine crystals are indicated with arrows.

can be distinguished. The distinct bipyramidal and needle forms can be readily identified as α- and β-polymorphs of glycine, respectively, in accordance with previous work.[21,22,26] The polymorphic nature of the other habits observed was established using Raman microscopy, from which we determined the "bladelike" crystals to be α-glycine[21] and the "brick-shaped" crystals to be β-glycine. The brick and blade shapes are visually distinguished by their cuboid and rhomboid habits, respectively.

In our experiments, we varied the flow rates of the glycine and the IPA streams in a systematic manner to examine the effect of these variables on the polymorphic selectivity of the formed glycine crystals. The other experimental variable we explored was the concentration of IPA in the antisolvent stream. In all of our experiments, the flow rates of antisolvent in the two side streams were kept equal at the chosen value to ensure that the focusing of the central stream consistently occurs in the middle of the channel. Below we present the results of these experiments arranged into three groups that involved (a) variation of flow rate, (b) variation of antisolvent composition, and (c) variation of both of these parameters.

Group I Experiments: Variation of Flow Rate at Constant Antisolvent Composition. In this group of experiments, we studied mainly the influence of the flow rate of streams in the microchannel on the polymorph selectivity of glycine while the compositions of the streams was maintained constant. Two different antisolvent compositions, 55% (series 1) and 70% (v/v) (series 2) of IPA in water, were used, with the volumetric flow rates of the streams varying between 0.2 and 2.0 mL/h. The flow rate of the glycine stream (center) was kept equal to that of each IPA stream on the side. By maintaining a constant ratio of the flow rates of the center and side streams, we ensured the width of the resulting focused stream (w_f) to be constant in all the experiments in this group. This constant focused stream width (before the liquid−liquid interfaces disappear due to diffusive mixing) eliminates variability in the diffusion time scales involved in the mixing of glycine and IPA streams. Using the available methods in microfluidic literature,[27] we estimate the w_f in these experiments to be about 53 μm.

Figure 3 shows the selectivity of glycine polymorphs observed in these experiments. In this figure we plot the

DOI: 10.1021/acs.cgd.5b00420
Cryst. Growth Des. 2015, 15, 3299−3306

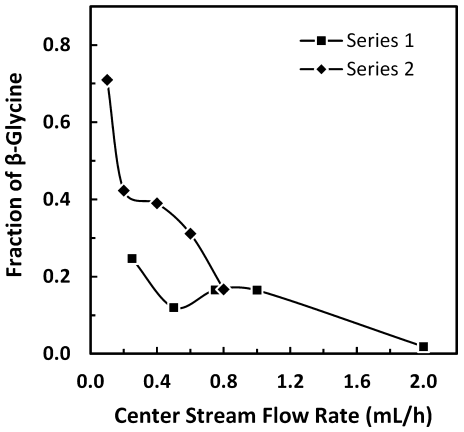

Figure 3. Polymorph selectivity of glycine crystals in group I experiments depicted as a function of stream flow rate: series 1 (■), 55% (v/v) IPA in water; series 2 (◆), 70% (v/v) IPA. The flow rate of the side stream for each condition was equal to that of the center stream. Each data point represents an average value obtained from five to seven populations of crystals. The error bars that represent the variability of the ordinate are smaller than the symbol in most cases and hence are not shown. The lines drawn are guides to the eye.

variation in the fraction of β-glycine crystals formed as a function of the flow rates of the streams. Note that we observed only two polymorphs in all of our experiments, α and β, but each at times occurred in different habits (see Figure 2). Hence, the sum of fractions of α- and β-glycine crystals is unity, and the trend in the fraction of α-glycine crystals complements that of β-glycine. In general, the fraction of β-glycine crystals formed decreased as the flow rate of the streams was increased. A higher concentration of IPA in the antisolvent stream resulted in a higher fraction of β-glycine crystals, and the effect of the flow rate was stronger when 70% (v/v) IPA was used as compared to the case of 55% (v/v) IPA. On the basis of the available solubility data on α-glycine crystals,[23−25] we estimate the degree of supersaturation achieved by completely mixed streams (S_e) to be 1.60 and 2.75, respectively, for antisolvent compositions of 55% IPA (series 1) and 70% IPA (series 2).

In our experimental setup, the glycine stream focused in the center of the microchannel is at a saturated condition, and the formation of crystals is induced by the supersaturation generated as a result of interdiffusion of species across the channel. The concentration gradients that drive the diffusion process are influenced by the convective (bulk) flow along the channel. The extent of diffusive mixing achieved in a given length of channel reduces as the convective flow increases.[6] Hence, as the flow rate of solutions increases, we expect the supersaturation gradients in the direction of flow to get "stretched". In general, as suggested by the Ostwald's rule of stages,[28] metastable crystal forms nucleate at relatively high degrees of supersaturation. In addition, low rates of generation of supersaturation promote the formation of the most stable polymorph.[15] On the basis of these observations, we expect increasing flow rates to reduce the formation of the metastable β-glycine crystals. Our results are indeed in agreement with this line of thought.

Group II Experiments: Variation of Antisolvent Concentration at Constant Flow Rate. The experiments in this group were focused on isolating the effect of rate of generation of supersaturation on polymorph selectivity. In these experiments we varied the IPA concentration in the antisolvent stream between 45% and 85% (v/v). Similar to the first group of experiments, the flow rates of the glycine stream and the IPA stream (each side) were kept equal, and two cases were studied, when all of the streams were flowing at 0.2 mL/h (series 3) and when they were at 0.5 mL/h (series 4). These experiments were performed at a constant w_f of ∼53 μm (the width of the focused center stream w_f depends only on the ratio of the flow rates of the center and side streams),[27] similar to that in the group I experiments described above.

Figure 4 shows the selectivity of glycine polymorphs observed in these experiments. In this figure we plot the

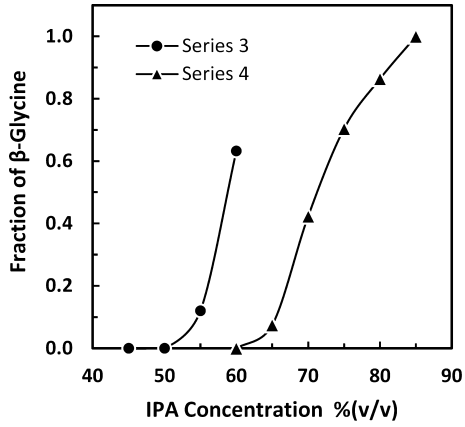

Figure 4. Polymorph selectivity of glycine crystals in group II experiments shown as a function of the strength of antisolvent: series 3 (●), 0.5 mL/h; series 4 (▲), 0.2 mL/h. The flow rates of all the streams are equal in a given series. Each data point represents an average value obtained from five to seven populations of crystals. The error bars that represent the variability in the ordinate are smaller than the symbol in most cases and hence are not shown. The lines drawn are guides to the eye.

variation in the fraction of β-glycine crystals formed as a function of the IPA concentration in the antisolvent stream and see a systematic variation in the fraction of β-glycine with increasing IPA concentration at a given flow rate of the streams. Moreover, the two sets of experiments (representing the two different flow rates of the streams) exhibit similar trends.

By varying the antisolvent concentration at a constant flow rate of streams, the degree of supersaturation is varied at each location in the microchannel under the same conditions of diffusion of species. As the strength of antisolvent is increased, we expect the degree of supersaturation generated to increase accordingly. We estimate S_e, defined above as the degree of supersaturation achieved in a completely mixed stream, to range from 1.17 (45% IPA) to 5.21 (85% IPA). The results from this group of experiments are in line with the common observation that high degrees of supersaturation generally produce metastable polymorphs. Analysis of these results from the perspective of the relative effects of mass transport and supersaturation on polymorph selectivity (in terms of Péclet number and net change in the supersaturation) is presented in a later section.

Group III Experiments: Variation of Both Flow Rate and Antisolvent Composition. In group I and II experiments, we attempted to decouple the influence of the flow rate of streams and the degree of supersaturation, respectively, on the polymorphic selectivity exhibited by the solute crystallizing in our microfluidic device. In group III experiments described

DOI: 10.1021/acs.cgd.5b00420
Cryst. Growth Des. 2015, 15, 3299−3306

here, this polymorphic selectivity was explored under the combined influence of these two parameters. Thus, we varied both the antisolvent composition and the flow rates of streams among these experiments. These experiments were carried out at three different IPA concentrations, 55%, 60%, and 70% (v/v), and the explored flow rates of streams were in the range of 0.1−0.7 mL/h. Table 1 lists the conditions of various

Table 1. Conditions Used in Group III Experiments

series	IPA conc. (% v/v)	glycine stream flow (mL/h)	IPA flow (each side) (mL/h)	focused stream width (μm)[a]	S_e
5	55	0.60	0.50	59.7	1.61
	55	0.50	0.50	53.3	1.60
	55	0.40	0.50	46.2	1.58
	55	0.30	0.50	38.1	1.51
6	55	0.70	0.40	74.3	1.57
	55	0.60	0.45	63.6	1.60
	55	0.40	0.50	46.2	1.58
	55	0.40	0.55	43.4	1.56
	55	0.30	0.60	33.6	1.44
7	60	0.30	0.50	38.1	1.88
	60	0.40	0.50	46.2	1.91
	60	0.50	0.50	53.3	1.90
	60	0.60	0.50	59.7	1.87
8	70	0.50	0.20	89.3	2.01
	70	0.40	0.20	79.8	2.18
	70	0.30	0.20	68.1	2.42
	70	0.20	0.20	53.3	2.75
	70	0.10	0.20	33.6	3.11

[a]The width of the focused center stream (w_f) was calculated from the ratio of the flow rates of the center and side streams, as described in the text. The degree of supersaturation attained by a completely mixed stream (S_e) is based on the solubility of α-glycine crystals.

experiments categorized into four series. In Figure 5 we compare the fraction of β-glycine crystals obtained in this group of experiments on the basis of the focused stream width w_f, a variable that is governed by the ratio of flow rates of center and side streams. For this plot, we estimated w_f under our experimental conditions from the relation obtained by Lee et al.[27] The observed trends in the fraction of β-glycine crystals show no particular pattern. This result emphasizes the complex dependence of the polymorph selectivity on local supersaturation gradients determined by the focused stream width and stream composition.

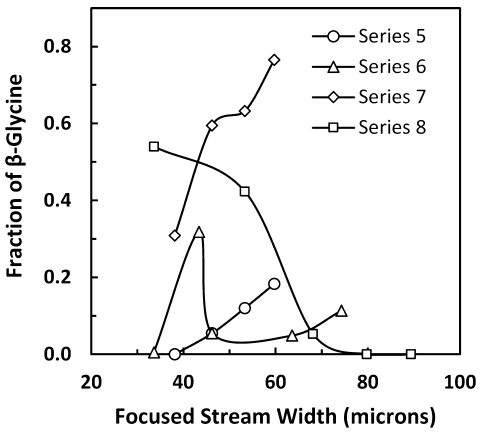

Figure 5. Polymorph selectivity of glycine crystals in group III experiments shown as a function of the width of the focused stream. The conditions of the experiments are given in Table 1. Each data point represents an average value obtained from five to seven populations of crystals. The error bars that represent the variability of the ordinate are smaller than the symbol in most cases and hence are not shown. The lines drawn are guides to the eye.

A Common Parameter for Polymorph Selectivity. Under steady-state conditions in a laminar flow regime present in our microfluidic device, all the volume elements of solution that flow along a particular streamline in the microchannel will experience the same variation in supersaturation. This supersaturation gradient varies by streamline. The various polymorphs collected at the end of the channel thus originate in the volume elements of solution that have experienced different supersaturation gradients. To estimate one such supersaturation gradient, we consider an elemental volume that flows along the center line of the channel. In our experiments, the incoming solute stream is saturated with glycine ($S = 1$). As the diffusive mixing of streams near the center of the channel causes the disappearance of the focused stream, the supersaturation of the volume element flowing along this center streamline changes to S_e. Thus, the net change in supersaturation along the channel (ΔS), given by ($S_e - 1$), gives us a typical supersaturation gradient experienced by the solution at each experimental condition.

As discussed earlier, increased convective flow in the microchannel adversely affects the degree of diffusive mixing achieved in a fixed length of the channel. The relative importance of convection to diffusion is expressed by the Péclet number (Pe), a dimensionless group that gives the order of the number of channel widths required for diffusive mixing.[6] Here we define the Péclet number as $Pe = (w_c U/D)$, in which w_c is the half-width of the channel (100 μm in our case), U is the average velocity of the stream, and D is the diffusion coefficient of the molecular species.

On the basis of the above considerations, to capture the combined effect of the degree of supersaturation and its spatial variation with diffusion on the polymorphic selectivity of a compound, we consider a dimensionless parameter λ of the form

$$\lambda = \Delta S^m Pe^n \quad (1)$$

Because increased ΔS promotes the nucleation of the metastable β-glycine polymorph and increased Pe adversely affects the formation of β-glycine, we anticipate the exponent m to be positive and n to be negative. For each experimental condition, we calculate ΔS on the basis of the solubility of α-glycine and the Péclet number using a value of 7.5×10^{-10} m^2/s for the diffusion coefficient of glycine.[18] The exponents m and n were chosen by trial and error. Since the exponent $-(2/3)$ often occurs in many correlations related to heat and mass transport processes, we have chosen the value of the exponent n that accompanies the Péclet number to be $-(2/3)$. Figure 6 shows a plot of the fraction of β-glycine crystals obtained as a function of λ with $m = 1$ and $n = -(2/3)$ for all of our experimental conditions (series 1−8). We note that for these chosen values of m and n, the majority of the data points follows a single trend (the notable exception being series 8, with also a few data points from series 4 and 7). Thus, the polymorphic selectivity exhibited by glycine crystals in most of the cases can be described by a single unifying parameter, λ.

DOI: 10.1021/acs.cgd.5b00420
Cryst. Growth Des. 2015, 15, 3299−3306

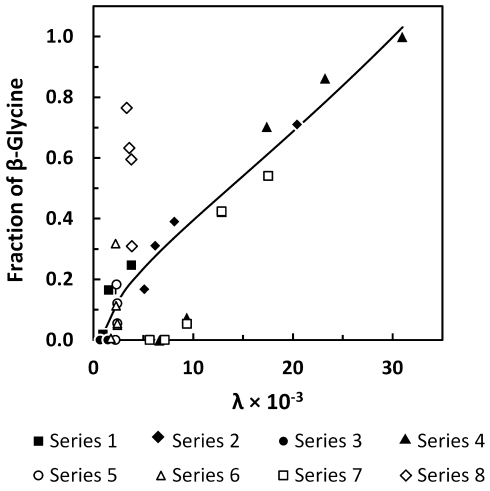

Figure 6. Polymorph selectivity of glycine crystals in all of the experiments (series 1–8) as a function of the parameter λ calculated from eq 1 using $m = 1$ and $n = -(2/3)$. The line drawn is a guide to the eye.

Given the simple definition of λ (eq 1), and in light of the complex supersaturation gradients that can manifest in the microchannel, the strong correlation we find between the polymorph selectivity and λ is interesting. To fully understand the influence of supersaturation gradients on the polymorphic outcome of crystallization, one needs a complete description of these gradients in the microchannel. A priori prediction of these gradients is difficult without a detailed modeling of the diffusion process within the channel. Below we present a finite element simulation of the concentration/supersaturation gradients in the microchannel for one of our experimental conditions

Modeling of Supersaturation Gradients in the Microchannel. We simulated the diffusive mixing of streams flowing in our microfluidic device using a finite elements solver (COMSOL Multiphysics v3.4). To simplify the computational effort, we modeled the convection/diffusion patterns only in the first 9 cm of the channel. To further alleviate the computational difficulties encountered, we employed a channel length of 3 cm with the volumetric flow rates scaled down by a factor of 3. Actual values were used for the remaining measurements of the channel geometry (such as width, height). Owing to the geometric symmetry of the channel, only half of the channel (from wall to center) was simulated. The diffusion of glycine and IPA was assumed to be isotropic, and typical values of 7.5×10^{-10} and 1.0×10^{-9} m^2/s were used as diffusion coefficients for glycine[18] and IPA, respectively. The volumetric flow rates simulated were 0.3 and 0.6 mL/h for the glycine stream and IPA stream, respectively. An antisolvent composition of 60% (v/v) IPA in water was used.

First, the velocity profile in the microchannel was obtained by solving the steady-state Navier–Stokes equation for the flowing streams. This velocity profile was then used in conjunction with the time-invariant (steady-state) convection–diffusion equation to obtain the concentration of glycine and IPA at various locations in the channel. Using these concentration values, the supersaturation at a given location was computed on the basis of the available solubility information on α-glycine in water–IPA mixtures.[23−25]

Panels a and b of Figure 7 show these supersaturation profiles across and along the microchannel, respectively. We observe that the degree of supersaturation varies significantly as

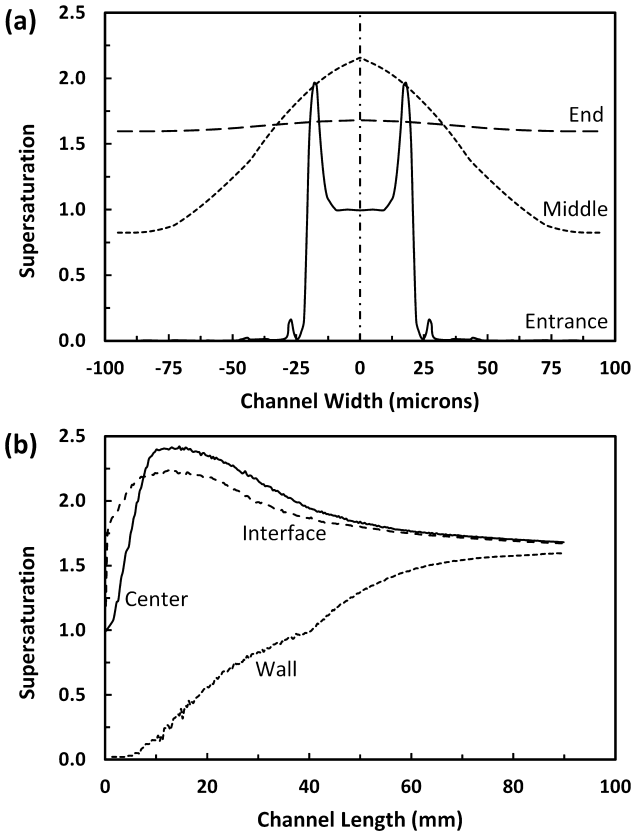

Figure 7. Calculated supersaturation profiles in the microchannel. (a) Supersaturation profile as a function of channel width at three locations: at the entrance to the channel, at 30 mm from the entrance (middle), and at 90 mm from the entrance (end). (b) Supersaturation profile as a function of length of the channel at three locations: near the wall, along the center line, and at the location where the liquid–liquid interface forms. Sharp variation in supersaturation with the location in the channel can be observed. S $(=C/C^*) < 1$ indicates an undersaturated solution.

a function of location within the channel. Figure 7a, which shows the variation of supersaturation across the channel, indicates that, near the entrance of the channel, sharp supersaturation gradients exist in the vicinity of the interface that defines the focused stream (about 19 μm from the center of the channel for the simulated experimental condition). As the solution flows down the channel, this interface disappears, and the supersaturation increases as a whole near the center before decreasing to a lower value. This rise and fall of supersaturation along the channel is also apparent from Figure 7b. We also note that, depending on the experimental conditions, a portion of the solution in fact can be undersaturated ($S < 1$) due to dilution. This wide spatial variation in the degree of supersaturation (coupled with the differences in the rate of change of supersaturation the solute molecules experience as they flow through the channel) potentially contributes to the formation of various polymorphs of a compound. This hypothesis is supported by the observed change in the polymorph selectivity exhibited by glycine crystals under different experimental conditions.

Unusual Habit of β-Glycine Crystals. Typically β-glycine crystals exhibit needlelike morphology.[26] However, in our experiments, we have also observed these β-glycine crystals to grow routinely with brick-shaped habit (see Figure 2). This brick shape for β-glycine is unusual. Upon the first observation,

DOI: 10.1021/acs.cgd.5b00420
Cryst. Growth Des. 2015, 15, 3299–3306

we established the polymorphic nature of the crystals through Raman spectroscopy. Torbeev et al.[21] reported this unusual habit for β-glycine crystals. By crystallizing glycine in the presence of tryptophan, these authors obtained prismatic β-glycine crystals similar to the bricklike morphology that we obtained. The fact that we consistently obtained these brick-shaped β-glycine crystals without introducing any foreign additives into the solution is significant.

In the results of experiments discussed above (Figures 3−5) the fraction of β-glycine crystals considered included both the needle-shaped and the brick-shaped β-glycine. From all these experiments, where appropriate, we have separately determined the fraction of the brick-shaped β-glycine crystals within the total β-glycine formed. In Figure 8 we plot the fraction of these

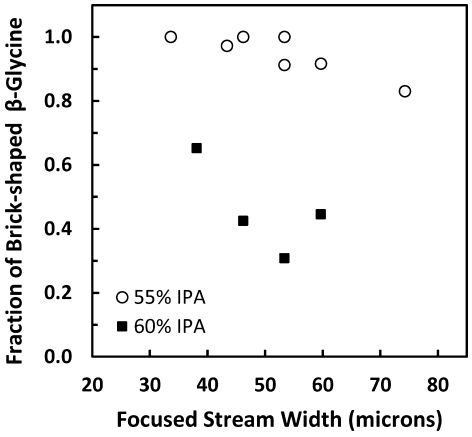

Figure 8. Habit modification of β-glycine crystals with experimental conditions expressed as the fraction of brick-shaped β-glycine crystals formed within the total population of β-glycine crystals. The results obtained with two antisolvent concentrations, 55% IPA (○) and 60% IPA (■), are shown. The data obtained with a particular antisolvent composition trend together when compared on the basis of the focused stream width.

brick-shaped β-glycine obtained in various experiments as a function of the focused stream width w_f. We note that data points obtained at a particular IPA concentration in the antisolvent stream trend together, with a lower IPA concentration resulting in a higher fraction of cubic β-glycine in general. The trends of the data depicted in Figure 8 indicate that the habit modification of β-glycine is related not only to the focused stream width, but also to the antisolvent concentration.

In traditional screening systems, crystal nucleation and growth typically occurs in a stagnant solution contained in a microbatch. In the microfluidic flow environment created in our platform, complex interplay between diffusion and convection of species occurs. The fact that crystal nucleation and growth in our experiments happen in a convective flow at the interface of different streams probably leads to the differences in the crystal habit observed. While the differences in the habits of crystals resulting from the experiments in our microfluidic platform are interesting, providing any explicit explanation for the observed habit modification of β-glycine crystals at this point would be purely speculative.

We have also observed that the aspect ratio of the formed bricks varied with experimental conditions, and in some cases these crystals resembled perfect "cubes". This observation suggests that the supersaturation gradients generated in our microfluidic device are also responsible for the change in the habit. The rate of generation of supersaturation may be a variable that can be explored to achieve habit control of crystals without the need of introducing foreign additives into the solution.

IV. CONCLUDING REMARKS

In this work, we presented an experimental technique of antisolvent crystallization in microchannels that enables us to explore the polymorph space of compounds in a straightforward and simple manner. This method also allows us to study the underlying processes that govern polymorph formation. The technique exploits the physics of diffusive mixing at the interfaces of solutions flowing in parallel layers, with the resulting dynamic gradients in supersaturation influencing the polymorph selectivity. We demonstrated the efficacy of the technique by influencing the crystallization of glycine into different polymorphs and crystal habits. We also identified an empirical correlation between the polymorph selectivity exhibited by glycine and a dimensionless parameter that captures the combined effect of supersaturation and variation in diffusion mixing. Further study would be needed to determine whether a parameter like λ can be used to predict crystallization outcomes in this or other similar systems.

Simulation of supersaturation gradients using a finite element solver shows that our experimental technique is capable of producing not only strong supersaturation gradients but also a wide range of degrees of supersaturation. Estimates of supersaturation experienced by the crystallizing solution at various locations of the microchannel indicate that the decoupling of nucleation and growth processes of crystals is possible with the proper selection of experimental conditions.

Some of our experiments consistently resulted in the formation of β-glycine crystals with unusual habits. The fact that we routinely obtained an unusual habit of β-glycine crystals in our microfluidic platform without using any additives for habit modification is interesting and highlights the influence of microscale physics on crystal nucleation and growth.

■ AUTHOR INFORMATION

Corresponding Author

*E-mail: kenis@illinois.edu.

Notes

The authors declare no competing financial interest.

■ ACKNOWLEDGMENTS

Financial support for this work was provided by the Agency for Science, Technology and Research (A*STAR), Singapore, and the National Institute of Health (NIH), USA (Grant No. 1 R21 GM075930-01). We thank Dr. Pedro López-Montesinos and Dr. Amit Desai for their help in COMSOL modeling. V.B. acknowledges Dr. Debangshu Guha, Eastman Chemical Company, for stimulating discussions regarding fluid flow and mass transport in microfluidic channels under the laminar flow regime. High-quality graphics from Microsoft Excel plots were generated using Daniel's XL Toolbox add-in for Excel (v 5.09), a free utility created by Daniel Kraus, Würzburg, Germany.

■ REFERENCES

(1) Bastin, R. J.; Bowker, M. J.; Slater, B. J. Salt Selection and Optimisation Procedures for Pharmaceutical New Chemical Entities. *Org. Process Res. Dev.* **2000**, *4*, 427−435.

DOI: 10.1021/acs.cgd.5b00420
Cryst. Growth Des. 2015, 15, 3299−3306

(2) Gardner, C. R.; Almarsson, Ö.; Chen, H.; Morissette, S.; Peterson, M.; Zhang, Z.; Wang, S.; Lemmo, A.; Gonzalez-Zugasti, J.; Monagle, J.; Marchionna, J.; Ellis, S.; McNulty, C.; Johnson, A.; Levinson, D.; Cima, M. Application of High Throughput Technologies to Drug Substance and Drug Product Development. *Comput. Chem. Eng.* **2004**, *28*, 943−953.
(3) Morissette, S. L.; Almarsson, Ö.; Peterson, M. L.; Remenar, J. F.; Read, M. J.; Lemmo, A. V.; Ellis, S.; Cima, M. J.; Gardner, C. R. High-throughput Crystallization: Polymorphs, Salts, Co-Crystals and Solvates of Pharmaceutical Solids. *Adv. Drug Delivery Rev.* **2004**, *56*, 275−300.
(4) Storey, R. A.; Docherty, R.; Higginson, P. D. Integration of High Throughput Screening Methodologies and Manual Processes for Solid Form Selection. *Am. Pharm. Rev.* **2003**, *6*, 100−105.
(5) Ware, E. C.; Lu, D. R. An Automated Approach to Salt Selection for New Unique Trazodone Salts. *Pharm. Res.* **2004**, *21*, 177−184.
(6) Squires, T. M.; Quake, S. R. Microfluidics: Fluid Physics at the Nanoliter Scale. *Rev. Mod. Phys.* **2005**, *77*, 977−1026.
(7) Hansen, C. L.; Skordalakes, E.; Quake, S. R. A Robust and Scalable Microfluidic Metering Method That Allows Protein Crystal Growth by Free Interface Diffusion. *Proc. Natl. Acad. Sci. U. S. A.* **2002**, *99*, 16531−16536.
(8) Zheng, B.; Roach, S. L.; Ismagilov, R. F. Screening of Protein Crystallization Conditions on a Microfluidic Chip Using Nanoliter-Size Droplets. *J. Am. Chem. Soc.* **2003**, *125*, 11170−11171.
(9) Laval, P.; Salmon, J.-B.; Joanicot, M. A Microfluidic Device for Investigating Crystal Nucleation Kinetics. *J. Cryst. Growth* **2007**, *303*, 622−628.
(10) Teychené, S.; Biscans, B. Microfluidic Device for the Crystallization of Organic Molecules in Organic Solvents. *Cryst. Growth Des.* **2011**, *11*, 4810−4818.
(11) Thorson, M. R.; Goyal, S.; Gong, Y.; Zhang, G. G. Z.; Kenis, P. J. A. Microfluidic Approach to Polymorph Screening through Antisolvent Crystallization. *CrystEngComm* **2012**, *14*, 2404−2412.
(12) Thorson, M. R.; Goyal, S.; Schudel, B. R.; Zukoski, C. F.; Zhang, G. G. Z.; Gong, Y.; Kenis, P. J. A. A Microfluidic Platform for Pharmaceutical Salt Screening. *Lab Chip* **2011**, *11*, 3829−3837.
(13) Goyal, S.; Thorson, M. R.; Schneider, C. L.; Zhang, G. G. Z.; Gong, Y.; Kenis, P. J. A. A Microfluidic Platfrom for Evaporation-Based Salt Screening of Pharmaceutical Parent Compounds. *Lab Chip* **2013**, *13*, 1708−1723.
(14) Goyal, S.; Thorson, M. R.; Zhang, G. G. Z.; Gong, Y.; Kenis, P. J. A. Microfluidic Approach to Cocrystal Screening of Pharmaceutical Parent Compounds. *Cryst. Growth Des.* **2012**, *12*, 6023−6034.
(15) He, G.; Bhamidi, V.; Wilson, S. R.; Tan, R. B. H.; Kenis, P. J. A.; Zukoski, C. F. Direct Growth of γ-Glycine from Neutral Aqueous Solutions by Slow, Evaporation-Driven Crystallization. *Cryst. Growth Des.* **2006**, *6*, 1746−1749.
(16) Knight, J. B.; Vishwanath, A.; Brody, J. B.; Austin, R. H. Hydrodynamic Focusing on a Silicon Chip: Mixing Nanoliters in Microseconds. *Phys. Rev. Lett.* **1998**, *80*, 3863−3866.
(17) Kenis, P. J. A.; Ismagilov, R. F.; Whitesides, G. M. Microfabrication inside Capillaries Using Multiphase Laminar Flow Patterning. *Science* **1999**, *285*, 83−85.
(18) Chang, Y. C.; Myerson, A. S. Diffusivity of Glycine in Concentrated Saturated and Supersaturated Aqueous Solutions. *AIChE J.* **1986**, *32*, 1567−1569.
(19) Duffy, D. C.; McDonald, J. C.; Schueller, O. J. A.; Whitesides, G. M. Rapid Prototyping of Microfluidic Systems in Poly-(dimethylsiloxane). *Anal. Chem.* **1998**, *70*, 4974−4984.
(20) Dawson, A.; Allan, D. R.; Belmonte, S. A.; Clark, S. J.; David, W. I. F.; McGregor, P. A.; Parsons, S.; Pulham, C. R.; Sawyer, L. Effect of High Pressure on the Crystal Structures of Polymorphs of Glycine. *Cryst. Growth Des.* **2005**, *5*, 1415−1427.
(21) Torbeev, V. Y.; Shavit, E.; Weissbuch, I.; Leiserowitz, L.; Lahav, M. Control of Crystal Polymorphism by Tuning the Structure of Auxiliary Molecules as Nucleation Inhibitors. The β-Polymorph of Glycine Grown in Aqueous Solutions. *Cryst. Growth Des.* **2005**, *5*, 2190−2196.
(22) Weissbuch, I.; Leiserowitz, L.; Lahav, M. "Tailor-Made" and Charge-Transfer Auxiliaries for the Control of the Crystal Polymorphism of Glycine. *Adv. Mater.* **1994**, *6*, 952−956.
(23) Yang, X.; Wang, X.; Ching, C. B. Solubility of Form α and Form γ of Glycine in Aqueous Solutions. *J. Chem. Eng. Data* **2008**, *53*, 1133−1137.
(24) Bouchard, A.; Hofland, G. W.; Witkamp, G.-J. Solubility of Glycine Polymorphs and Recrystallization of β-Glycine. *J. Chem. Eng. Data* **2007**, *52*, 1626−1629.
(25) Orella, C. J.; Kirwan, D. J. Correlation of Amino Acid Solubilities in Aqueous Aliphatic Alcohol Solutions. *Ind. Eng. Chem. Res.* **1991**, *30*, 1040−1045.
(26) Seyedhosseini, E.; Ivanov, M.; Bystrov, V.; Bdikin, I.; Zelenovskiy, P.; Shur, V. Y.; Kudryavtsev, A.; Mishina, E. D.; Sigov, A. S.; Kholkin, A. L. Growth and Nonlinear Optical Properties of β-Glycine Crystals Grown on Pt Substrates. *Cryst. Growth Des.* **2014**, *14*, 2831−2837.
(27) Lee, G.-B.; Chang, C.-C.; Huang, S.-B.; Yang, R.-J. The Hydrodynamic Focusing Effect inside Rectangular Microchannels. *J. Micromech. Microeng.* **2006**, *16*, 1024−1032.
(28) Bernstein, J. *Polymorphism in Molecular Crystals*, 1st ed.; Oxford University Press: New York, 2002.

DOI: 10.1021/acs.cgd.5b00420
Cryst. Growth Des. 2015, 15, 3299−3306